Probe size effects on the microrheology of associating polymer solutions

Qiang Lu and Michael J. Solomon
Department of Chemical Engineering and Macromolecular Science and Engineering Program, University of Michigan, Ann Arbor, Michigan 48109-2136

(Received 7 May 2002; revised manuscript received 8 August 2002; published 20 December 2002)

Diffusing wave spectroscopy has been used to investigate the thermally driven displacement of colloidal particles dispersed in solutions of associating polymers (APs). The effect of varying colloidal probe size on the measured particle displacements is studied in particular. Recent theories of microrheology are examined in light of the observed effects. The associating polymer used in this research was a linear polyethylene oxide (PEO) chain (molecular weight 35 000 g/mole) with a Cl_{14} aliphatic group appended to each end of the PEO. Above a critical concentration, the associating polymers display linear viscoelasticity consistent with the Maxwell model. The concentration of aqueous AP solutions was varied from 0.25 to 4.0 wt. %. At low concentration of APs, the mean square displacement of the colloidal beads was indistinguishable from simple Brownian diffusion in the aqueous solvent. However, at concentrations greater than 0.5 wt. %, the mean square displacement differed from simple diffusion in a way that was found to be consistent with the Maxwell model linear viscoelasticity (LVE) of the AP solutions. Significantly, for the most concentrated solutions, as the probe particle size was varied from 0.3 to 2.2 μm, the observed mean square displacement deviated substantially from the generalized Stokes-Einstein behavior predicted by microrheological theories. Our experiments showed that these deviations could not be attributed to specific physicochemical interactions at the probe-matrix interface, since observed mean square displacements were independent of different probe surface chemistries studied. Moreover, this particle size effect was not observed in semidilute, high molecular weight PEO solutions (molecular weight 4.0×10^6 g/mole). We concluded that possible effects of AP network compressibility and AP depletion at the probe surface could not account for the observed particle size effects. We examined recent reports of the structural heterogeneity in AP solutions for their possible connection to our observation of the breakdown of the generalized Stokes-Einstein equation for this system. Numerical conversion of the microscopic results to the linear viscoelastic moduli, $G'(\omega)$ and $G''(\omega)$, by means of a constrained regularization method (CONTIN), demonstrates that the experiments with larger probe particles are most consistent with the single-mode Maxwell model LVE observed by macroscopic mechanical rheology.

DOI: 10.1103/PhysRevE.66.061504 PACS number(s): 83.10.Pp, 83.60.Bc, 82.70.Dd

I. INTRODUCTION

Microrheology is a class of methods in which material viscoelasticity is characterized by quantifying the local displacement of embedded colloidal beads in response to an applied force, and converting the displacement of the probe beads to macroscopic material properties, such as linear viscoelasticity [1–4]. The thermally driven displacement of particles in viscoelastic fluids has been of long-standing interest [5–10]. In the long time limit, deviations from Stokes-Einstein behavior for probe diffusion in polymer solutions have been observed [6–8]. Microrheology builds on this early work by considering the time-dependent diffusivity of probe particles and providing a formalism to pass from measurement of diffusion to characterization of rheology of the material at the microscopic level. In microrheology, the driving force is either thermal fluctuations [1,2] or an external force, usually of magnetic [11] or optical [12] origin. One of the advantages of microrheology is that this method can be applied when only a small volume of fluid is available. In addition, since microrheology measures material properties at the microscopic level, it is capable of probing local viscoelastic properties, which cannot be otherwise quantified by traditional rheological measurements. Moreover, the maximum frequency to which the linear viscoelastic response can be characterized may be orders of magnitude greater with microrheology than with mechanical rheology. Microrheological studies of actin solutions [4,13], cells [11], semidilute solutions of flexible polymers [3], colloidal suspensions and emulsions [2], and micellar systems [14,15] have all been recently reported. For additional references, refer to recent reviews of Gisler and Weitz [16], MacKintosh and Schmidt [17], Mukhopadhyay and Granick [18], Solomon and Lu [19], and Harden and Viasnoff [20].

Experimentally, microrheology relates the mean square displacement, $\langle \Delta r^2(t) \rangle$, of colloidal particles to the linear viscoelastic response of the material in which they are dispersed. $\langle \Delta r^2(t) \rangle$ can be measured by a number of different experimental techniques. Epifluorescence microscopy [21], laser deflection particle tracking [3], optical interferometry [4], atomic force microscopy [22], dynamic light scattering [23], and diffusing wave spectroscopy [1,2] have all been used. Diffusing wave spectroscopy (DWS) is a multiple scattering technique in which fluctuations of intensity transmitted or backscattered from a turbid sample are related to the displacement of scattering objects. With DWS, $\langle \Delta r^2(t) \rangle$ can be extracted from the measured intensity autocorrelation function, $g_{(2)}(t)$, by means of the theory of Pine, Weitz, and co-workers [24,25]. DWS is well suited to microrheology due to its excellent temporal and spatial resolution: these limits are approximately 10^{-6} s and 10^{-1} nm, respectively [2].

Microrheology supposes the validity of the generalized Stokes-Einstein equation [2]. Here the generalization refers to the extension of the Stokes-Einstein equation valid for Newtonian fluids to one valid for viscoelastic fluids with frequency-dependent linear viscoelastic moduli. A number of assumptions are required to apply the generalized Stokes-Einstein equation. First, the implanted probes are assumed to be spherical, monodisperse, dilute, and noninteracting. In addition, the size of the beads must be large relative to the characteristic length scale of the material structure so that the assumption of continuum viscoelasticity is valid [4,26]. Finally, it is assumed that the probe beads do not affect the existing structure of the complex fluid in which they are dispersed by inducing structural inhomogeneity either in the bulk material or in the vicinity of the probe surfaces.

To date, the range of validity of these assumptions has not been fully tested. In this study, we carry out a series of microrheological experiments in a complex fluid with Maxwell model linear viscoelasticity. In these studies the size and surface chemistry of the colloidal probes are systematically varied. By investigating the behavior of these probe particles, especially on very short time and length scales, we hope to improve our understanding of the range of the validity of the generalized Stokes-Einstein equation. Note that although probe size effects have been investigated for complex fluids in the long time limit [27,6–8], such effects in viscoelastic solutions that are relevant to microrheology have not been studied before.

Other recent studies have investigated the limits of microrheology. Schnurr *et al.* [4] recognized that at low frequencies, for complex fluids that could be modeled as a compressible polymer network viscously coupled to a Newtonian fluid, the generalized Stokes-Einstein equation may not hold. This effect was quantitatively investigated by Levine and Lubensky using a two-fluid model [28]. By comparing the linear response of a sphere dispersed in the two-fluid viscoelastic matrix, Levine and Lubensky were able to precisely quantify the range of validity of the generalized Stokes-Einstein equation. In addition, Crocker *et al.* [21] have recently developed a two-particle microrheology method, which measures the linear viscoelasticity (LVE) of locally inhomogeneous viscoelastic materials by cross correlating the thermal motion of pairs of probe beads.

To explore the limits of microrheology, we chose to investigate the effect of probe size in a system with model linear viscoelastic properties. We selected associating polymer solutions as such a model system, because they display ideal Maxwell model linear viscoelasticity [29,30]. In addition, the dynamics of colloidal particles in associating polymer solutions are of interest in their own right: applications in paints [30], drilling fluids [31], and genomic sequencing [32] are all related to such behavior.

Telechelic associating polymers (APs) are linear polymers with chain ends of different chemical functionality than the remainder of the molecule. Typically, the main chain is chosen to be hydrophilic and the chain ends are modified to be hydrophobic. When such an AP is dissolved in water, the hydrophobic chain ends tend to associate together to form micellelike aggregates. If the polymer concentration is high enough, a physically crosslinked network structure is formed [29]. The association of chain ends leads to unusual rheological properties, such as single-mode Maxwell model linear viscoelasticity, strong enhancement of the zero-shear viscosity, shear thinning and, sometimes, shear thickening [33,34]. Reviews of the unique physicochemical and rheological properties of associating polymers have been published by Winnik and Yekta [30] and Larson [35]. It has been discovered that the characteristic Maxwell relaxation time corresponds to the time for detachment of one-polymer chain from a hydrophobic aggregate [29,33,34]. The characteristic pore size of the network, which is relevant to the diffusion of dispersed particles, is controlled by polymer molecular weight, aggregation behavior, and concentration [29,36]. Associating polymer systems have also been used as model systems to study equilibrium clustering and dynamic transitions. Measurements of probe diffusion can also be compared to simulations to study the underlying structure of the associating polymer solutions [37].

An advantage of the AP model system is that its linear viscoelastic storage and loss moduli, $G'(\omega)$ and $G''(\omega)$, satisfy the single-mode Maxwell model. Microrheology requires complex data reduction schemes including numerical Laplace transformation, analytical continuation and/or inverse transformation of integral equations [1–3]. For a fluid with ideal Maxwell model linear viscoelasticity, these results can be obtained analytically. Thus, experiment and theory can be compared at intermediate stages and the performance of the various numerical conversion methods can be systematically evaluated.

In this research, we used diffusing wave spectroscopy to quantify the mean square displacement of colloidal probes dispersed in the AP solutions. The effects of the probe bead diameter, polymer concentration, and probe surface chemistry of the beads were investigated. The performance of the generalized Stokes-Einstein equation is discussed in terms of the polymer network structure, probe surface depletion, and probe-polymer interactions. The linear viscoelastic storage and loss moduli obtained by microrheology are compared to those measured by traditional mechanical rheology.

II. THEORETICAL BACKGROUND OF SINGLE-PARTICLE MICRORHEOLOGY

Theories of microrheology relate the microscopic displacement of embedded probe particles to the macroscopic linear viscoelasticity of the complex fluid. A number of treatments of the theoretical basis for extracting the linear viscoelasticity from such microscopic measurements of probe displacement are available. Based on a generalized Langevin equation with a memory function and the assumption of the generalized Stokes-Einstein relationship, Mason and coworkers [1,2] related the Laplace transformed modulus $\tilde{G}(s)$ to $\langle \Delta\tilde{r}^2(s)\rangle$, which is the Laplace transform of $\langle \Delta r^2(t)\rangle$, a quantity that can be directly measured,

$$\tilde{G}(s)=\frac{k_BT}{\pi as\langle \Delta\tilde{r}^2(s)\rangle}. \tag{1}$$

Here a is the radius of the probe particles and k_BT is the thermal energy. To arrive at Eq. (1), the following assumptions were made: First, the Stokes-Einstein equation valid for Newtonian fluid was generalized to viscoelastic fluids with frequency-dependent linear viscoelastic moduli; Second, continuum viscoelasticity was assumed; Third, inertial effects of the probe beads were neglected.

Once $\tilde{G}(s)$ has been obtained from $\langle \Delta r^2(t) \rangle$, methods such as analytical continuation [2], relaxation spectra [3], conversion of creep compliance [38], or CONTIN deconvolution [19] are available to extract the desired linear viscoelastic moduli, $G'(\omega)$ and $G''(\omega)$.

Other microrheological methods have been developed which do not rely on the measurement of the mean square displacement to extract linear viscoelastic properties. Schnurr *et al.* [4] studied the viscoelasticity of flexible and semiflexible polymer networks, by monitoring thermal fluctuations of the probe beads using laser interferometry. In this case the particle motion was characterized by the power spectral density (PSD) of the probe displacement. This PSD approach has also been used by Popescu and co-workers [23]. By means of the fluctuation-dissipation theorem, the PSD of probe displacement was related to the imaginary part of the complex compliance. The viscoelastic quantities, such as storage and loss moduli are then obtained from the complex compliance. Although this method avoids complicated data reduction schemes necessitated by Eq. (1), it has yet to be applied to the analysis of DWS results, most likely because the conversion from $\langle \Delta r^2(t) \rangle$ to the PSD is itself difficult. Here, we limit our efforts to the application of Eq. (1).

III. MATERIALS AND EXPERIMENTAL METHODS

A. Associating polymers

The associating polymer, hydrophobically modified ethoxylated urethane (HEUR) was synthesized by a modification of the procedure of Kaczmarski and Glass [39]. Polyethylene oxide (PEO) of molecular weight 35 000 g/mole and polydispersity 1.18 (Fluka, Milwaukee, WI) was used. PEO was first purified by azeotropic distillation to remove any residual water; 50 g PEO was dissolved in the mixture of 150 ml toluene (Sigma Aldrich, WI) and 150 ml tetrahydrofuran (Fluka). At 49 ± 1 °C and in an N_2 atmosphere, 100-equiv excess of isophorone diisocyanate, and 0.2 wt. % (based on total polymer weight) of the catalyst dibutyltin dilaurate were added to the PEO solution. The reaction proceeded for 3.5 h before an additional 0.2 wt. % (based on total polymer weight) of dibutyltin dilaurate was added, along with 120 equiv of 1-tetradecanol. The reaction was continued at 49 ± 1 °C for an additional 4 h. The solution was then slowly transferred into 500 ml of petroleum ether. Precipitation occurred upon stirring for at least 1 h. The precipitate was collected with a Buchner funnel and then dissolved into warm acetone. After the filtration of the warm polymer-acetone solution, the polymer was again precipitated into petroleum ether. The petroleum ether was then filtrated and the finished HEUR polymer was collected.

Mechanical rheological measurement was performed on the polymers made according to the above mentioned synthetic protocol. The linear viscoelastic properties were plotted in Fig. 1. The experimental data were fit to a single-mode Maxwell model. The plateau modulus and relaxation time were found to be 205 Pa and 0.017 s^{-1}, respectively.

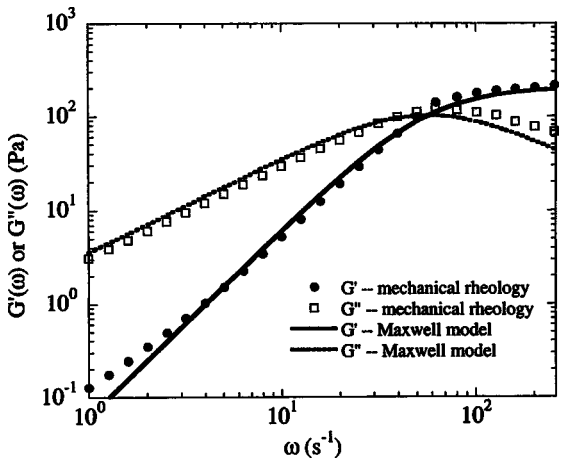

FIG. 1. $G'(\omega)$ and $G''(\omega)$ measurements of 4.0 wt. % associating polymer solutions collected by time-temperature superposition are reported at a reference temperature $T = 25$ °C. The curve is the best fit of a single-mode Maxwell model. The extracted plateau modulus G and relaxation time τ are reported in Sec. III A. The associating polymer is a PEO backbone (molecular weight 35 000 g/mole) with a C_{14} aliphatic group appended to each end of the backbone by an isophorone diisocyanate linker.

B. Colloidal probe beads

Both unmodified monodisperse polystyrene and carboxylate-modified particles were studied (Seradyn Inc., Indianapolis, IN). As reported by the manufacturer, the unmodified polystyrene (PS) particles were synthesized by emulsion polymerization in the presence of small mount of surfactant. Carboxyl-modified PS particles were made by a similar process, except that additional acrylic acid groups were copolymerized with styrene during the emulsion polymerization. The size of the particles ranged from 0.3 to 2.2 μm. Monodispersed colloidal silica beads ($a = 0.25$ μm) were synthesized by the method of Stober, Fink, and Bohn [40] and Bogush, Tracy, and Zukoski [41]. The volume fraction of the probe suspension was confirmed by measurement of the solid content. The diameter of all probe beads was characterized by means of dynamic light scattering of dilute samples.

C. Diffusing wave spectroscopy

1. Sample preparation

Dry HEUR samples were dissolved in deionized water at the desired weight fraction. To ensure complete dissolution, samples were maintained at 60 °C for 24 h. Polymer solutions were used within a week of preparation.

Aqueous probe particle solution (at 2.0 vol %) were added to an equal volume of stock HEUR solutions prior to measurement. The mixture was heated to 60 °C, vortex mixed, and then heated for another 0.5 h to ensure complete mixing.

TABLE I. Comparison of l^* values calculated from both Mie theory and DWS measurements (for dilute aqueous suspension of colloidal particles).

Particle size	Particle concentration	Mie theory	DWS measurements
0.6 μm	1.0%	0.22 mm	0.22 mm
	2.0%	0.11 mm	0.11 mm
1.1 μm	1.0%	0.29 mm	0.32 mm
	2.0%	0.14 mm	0.16 mm
2.2 μm	1.0%	0.45 mm	0.47 mm
	2.0%	0.22 mm	0.23 mm

The mixture was transferred to rectangular cuvettes for DWS measurements. The concentration of probe particles was 1.0 vol % for all experiments.

2. DWS experiments

DWS measurements were carried out in transmission mode on an ALV compact goniometer (Langen, Germany). The wavelength of the incident laser light was $\lambda = 488$ nm (Innova I-70, Coherent Inc., Santa Clara, CA). The incident laser beam was propagated through a lens and focused on the front surface of the sample. Dual avalanche photodiode detectors were positioned in the transmission mode to collect the scattered light. The detector output was then sent to a digital correlator and the normalized intensity autocorrelation function $g_{(2)}(t) = \langle I(0)I(t)\rangle / \langle I\rangle^2$ was constructed by cross correlating the signal from the two detectors [2], where $I(t)$ is the scattering intensity at time t and $\langle\,\rangle$ denotes a time average. The temperature was controlled at $T = 25\,^{\circ}$C. To ensure the validity of the diffusive light approximation for interpretation of diffusing wave spectroscopy data, the sample thickness must be at least several times the mean free transport length l^* [24]. This condition was satisfied for the 2 mm thickness of the sample cells used.

The conversion from $g_{(2)}(t)$ to mean square displacement requires knowledge of the mean free transport length l^*. l^* characterizes the distance over which the direction of propagation of the incident light is randomized due to multiple scattering. It is a function of the concentration of probes and the ratio of the probe refractive index to the matrix refractive index. For dilute probe solutions it can be computed by Mie theory [42]. Note that although the matrix refractive index is a function of concentration for our test solutions, for the low polymer concentrations studied here the change is no greater than 0.3%, so we use the refractive index of water ($n = 1.33$) for l^* calculations. To further confirm our l^* calculations, we also extracted l^* by applying the multiple scattering theory of Weitz and Pine [24] to DWS measurement of dilute, noninteracting suspensions. Table I lists l^* values calculated from both Mie theory and measured experimentally by DWS. The results are in good agreement. Thus, we use the value of l^* computed from Mie theory for all measurements reported here.

The duration of DWS measurements varied from 3 to 24 h for results reported here. For low viscosity solutions, samples were resuspended every 10 min to avoid possible effects of sedimentation [24]. For the associating polymer solutions studied here, resuspension was not required due to the high viscosity of the solutions, which were typically hundreds of times more viscous than water. In addition, our tests with one sample for periods of 8, 12, and 24 h showed no sedimentation effects on correlation functions collected. DWS results were reproducible over a period of several weeks, after which the associating polymer gradually degraded.

D. Data analysis

1. Mean square displacement extraction

First, $g_{(2)}(t)$ is related to the normalized electric autocorrelation function $g_{(1)}(t)$ by the Siegert relation: $g_{(2)}(t) = 1 + \beta|g_{(1)}(t)|^2$, where β is an instrument constant. In this study, β was determined by one of the two methods: A semilogarithmic extrapolation procedure as described by Johnson and Gabriel [43] or by averaging the first thirty data points of the data set. The methods gave equivalent results and thus were used interchangeably. According to the Weitz and Pine theory [24] for the diffusive light approximation, $g_{(1)}(t)$ can be expressed for a point source illumination as

$$g_{(1)}(t) = \int_Q^\infty D(\varepsilon,\xi,\zeta)\,\xi e^{-(1-\zeta)\xi} d\xi. \tag{2}$$

Here ε and ζ are dimensionless parameters that are functions of (l^*/L). L is the thickness of the sample and l^* is the transport mean free path. D is a function of ε, ξ, and ζ, as reported by Weitz and Pine [24]. Therefore, once $g_{(1)}(t)$ is available from DWS measurement, the lower integration limit Q can be extracted by performing a nonlinear least squares fit of Eq. (2). Q is related to $\langle \Delta r^2(t)\rangle$ through its definition: $\langle \Delta r^2(t)\rangle = Q k_0^{-2}(L/l^*)^{-2}$, where k_0 is the wave vector of the incident light, $k_0 = 2\pi n/\lambda_0$. To maintain consistency in data analysis, we analyzed all data for which $g_{(2)}(t) \geqslant 0.01$. Below this limit, background fluctuations, most likely due to the laser source, contributed systematic error. For our systems, the magnitude of these background fluctuations was never greater than about 0.005.

2. Extraction of $G(s)$ from $\langle \Delta r^2(t)\rangle$

To apply Eq. (1) to compute $G(s)$ we require the Laplace space mean square displacement $\langle \Delta \tilde{r}^2(s)\rangle$. A number of methods to perform the conversion are available [2,3,38]. Although other methods might be equally acceptable, here we choose to perform the Laplace transformation numerically. We assess the accuracy of the numerical transformation, particularly with regards to the range of s for which the limited range of time domain data allows a valid transformation, by analyzing results for an analytical function that corresponds to the single-mode Maxwell model [15]. We find that the minimum time resolution of our results ($\tau_{\min}$) allows $s_{\max} \approx 0.1\tau_{\min}^{-1}$ with an error of no more than 10%. $s_{\min}$ is determined by the longest delay time of the correlation function. This maximum delay time is determined by the dynami-

cal and optical properties of the individual sample. We find $s_{\min} \approx 10\tau_{\max}^{-1}$, where $\tau_{\max}$ is the maximum delay time of a particular DWS spectra. This cutoff yields an error at $s_{\min}$ of no more than 2%. These errors, computed for an analytical function, are representative of errors due to the numerical Laplace transformation of the experimental data.

3. LVE construction from $G(s)$ using CONTIN

The frequency domain $G'(\omega)$ and $G''(\omega)$ were obtained by application of the inversion routine of Provencher [44,45]. Application of this transformation method in microrheology has been discussed by Solomon and Lu [19]. We proceed by expressing the relaxation spectra as a summation of Maxwell modes, a procedure that is valid for any viscoelastic fluid [46]. Thus, the shear modulus $G_r(t) = \Sigma_i^N G_i e^{-t/\tau_i}$, where G_i is the amplitude and τ_i is the relaxation time of mode *i*. The Laplace domain shear modulus $\tilde{G}(s)$ can be expressed as [3]

$$\tilde{G}(s) = \sum_j^N \frac{G_j s}{s + 1/\tau_j}. \tag{3}$$

$\tilde{G}(s)$ is available from experiments as per the previous sections and application of Eq. (1). The problem is then to determine the G_i and τ_i parsimoniously. CONTIN is a general purpose constrained regularization method developed for solution of inverse problems of this kind [44,45]. It has found wide application in the areas of dynamic light scattering [47] and rheology [48]. Here we describe the details of its application to microrheology.

When Eq. (3) is applied to Provencher's CONTIN objective function we obtain the following minimization equation:

$$\sum_{j=1}^{M} w_j \left[\tilde{G}(s_j) - \sum_{i=1}^{N} \frac{G_i s_j}{s + 1/\tau_i} \right]^2 + \alpha^2 \sum_{j=1}^{N_{\text{reg}}} \left[r_j - \sum_{i=1}^{N} R_{ij} G_i \right]^2 = A. \tag{4}$$

Here, w_j is a weighting factor and α is the regularization parameter that controls the degree of regularization. r_j and R_{ij} are regularization arrays of dimension $N_{\text{reg}} \times 1$ and $N_{\text{reg}} \times N$, respectively, which are constructed according to Provencher [44,45]. A is the objective parameter to be minimized. Typically the weighting factors w_j are unbiased and α is chosen according to a Fisher F test that determines a probability for rejection of oversmoothed solutions [44,45]. The quality of the CONTIN fit was assessed by analysis of the residual difference between the fit and data, as discussed in Sec. IV C. To determine the sensitivity of the fit, we examined the effect of varying regularization factor α and weighting factor w_j for experimental data and a model system constructed from a multimode Maxwell model. The CONTIN algorithm was able to construct LVE of both systems with low residual error. While the quality of CONTIN fit is sensitive to these parameters, the sensitivity is equivalent to that typically observed in other applications of CONTIN, such as dynamic light scattering [47]. Once G_i and τ_i are determined, the linear viscoelastic moduli were constructed by means of standard expressions [46].

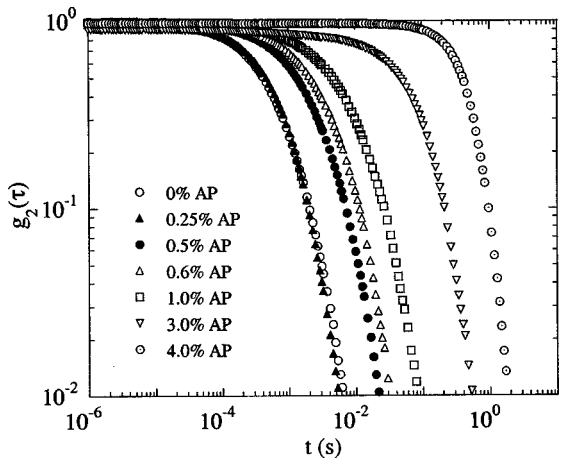

FIG. 2. DWS intensity autocorrelation functions of associating polymer solutions at various concentrations are plotted vs time. The probe beads have a diameter of 2.2 μm. Probe concentration is fixed at 1.0 vol %. Results are for $T = 25\,^\circ$C.

E. Mechanical rheology

The mechanical rheology of APs was measured using a AR 1000 constant stress rheometer (TA instruments, New Castle, DE) and an ARES strain-controlled rheometer (Rheometrics Scientific Inc., Piscataway, NJ). For the AR 1000 rheometer, the frequency range was $0.01\ \text{s}^{-1} < \omega < 300\ \text{s}^{-1}$. Temperature was controlled by a Peltier plate to $\pm 0.01\,^\circ$C. For the ARES rheometer, the frequency range is $0.01\ \text{s}^{-1} < \omega < 100\ \text{s}^{-1}$. Temperature was controlled by a water bath to $\pm 0.1\,^\circ$C.

IV. RESULTS AND DISCUSSION

A. DWS investigation of AP solutions

The effect of associating polymer concentration on the thermal motion of colloidal probes was investigated. The concentration range on a weight basis was from 0 wt. % AP (pure probe particle solution) to 4.0 wt. % AP. Figure 2 plots DWS $g_{(2)}(t)$ of AP-colloidal probe solutions. The probe particle size is 2.2 μm. At very low concentration (i.e., AP concentration $\leqslant$0.25 wt. %), the $g_{(2)}(t)$ curve nearly overlays that of pure water, indicating that AP has no effect on $g_{(2)}(t)$ at this concentration. With further increase of polymer concentration, the decay time of $g_{(2)}(t)$ shifts to longer times. This shift indicates a retardation of probe dynamics in the AP solutions. Presumably, such retardation occurs concomitantly with the formation of network structure in the AP solutions.

$g_{(2)}(t)$ was converted to $\langle \Delta r^2(t) \rangle$ (Fig. 3) by the methods described in Sec. III D 1. Again, at low concentration, the almost identical $\langle \Delta r^2(t) \rangle$ curves indicate that the probe bead displacement is hardly affected by the presence of the associating polymer solutions. In addition, the slope of the $\langle \Delta r^2(t) \rangle$ curve on log-log coordinates is nearly 1. This scaling indicates that the dynamics of the embedded beads are

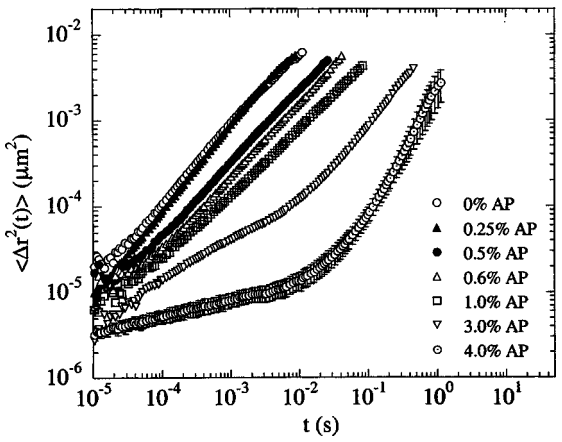

FIG. 3. $\langle \Delta r^2(t) \rangle$ of different polymer concentrations are calculated from the data of Fig. 2 and plotted vs time. The standard deviation of four runs of experiments on 2.2 μm probe in 4.0 wt. % AP solutions is also plotted.

diffusive over the full range of time probed.

Above polymer concentrations of 0.5%, the shape of the $\langle \Delta r^2(t) \rangle$ curve progressively changes. At high concentrations, the $\langle \Delta r^2(t) \rangle$ curve is characterized by a nearly constant value at short times followed by a crossover to diffusive behavior (i.e., slope of 1 on a log-log scale) at long times. These results are consistent with the $\langle \Delta r^2(t) \rangle$ curve predicted from a single-mode Maxwell model in the absence of inertial effects [15],

$$\langle \Delta r^2(t) \rangle = \frac{k_B T}{\pi a G}(t/\tau + 1). \tag{5}$$

Here G is the plateau modulus and τ is the relaxation time. The range of validity of this equation is the same as that of Eq. (1). Therefore, $\langle \Delta r^2(t) \rangle$ of the model associating polymer solutions at high concentrations is consistent with the Maxwell model prediction. Hence, we conclude that the network structure has formed at these conditions, since there is ample evidence that the onset of Maxwell model behavior signals the network formation in the AP solutions [29].

To assess the effect of sample preparation, measurement, and data analysis error on mean square displacement results, one sample (2.2 μm probe particles in 4.0 wt. % AP solutions) was selected for in-depth analysis. We conducted four independent experiments. The mean and standard deviation of the data are plotted in Fig. 3.

In addition, a simple check confirms that the microscopic $\langle \Delta r^2(t) \rangle$ data are consistent with the results of mechanical rheology. The zero-shear viscosity η_0 can be extracted from linear viscoelastic measurements with mechanical rheology because $\eta_0 = [G''(\omega)/\omega]_{\omega \to 0}$. Equivalently, $\eta_0 = [t/J(t)]_{t \to \infty}$, where $J(t)$ is the creep compliance. Note that $J(t)$ is also proportional to the $\langle \Delta r^2(t) \rangle$ of the probe particles according to Mason, Gang, and Weitz [2]. Table II shows that the results of DWS measurements and mechanical rheology are in good agreement for both 2% and 4% AP solutions.

TABLE II. Comparison of zero-shear viscosities obtained from probe mean square displacement and mechanical rheology.

	2.0% AP	4.0% AP
η_o, Mechanical rheology	0.31 Pa s	1.91 Pa s
η_o, Microrheology	0.29 Pa s	1.65 Pa s

B. Effect of particle size on $\langle \Delta r^2(t) \rangle$

We investigated the $\langle \Delta r^2(t) \rangle$ of probe particles of varying diameters at fixed polymer concentration to assess the validity of the generalized Stokes-Einstein equation for the associating polymer system.

We recognized that, according to Eq. (1), and due to the fact that $\tilde{G}(s)$ is a material property independent of probe particle size, the product $(\langle \Delta \tilde{r}^2(s) \rangle a)$ must be independent of the particle size. Hence, $\langle \Delta r^2(t) \rangle$, the Laplace transform pair of $\langle \Delta \tilde{r}^2(s) \rangle$, will likewise exhibit the same a^{-1} scaling. This scaling is easily confirmed to be consistent with the case of simple diffusion in Newtonian fluids. Thus, by plotting the product $(\langle \Delta r^2(t) \rangle a)$ versus time for various particle sizes, deviation from a universal master curve indicates a deviation from the behavior predicted by Eq. (1).

Figure 4 shows that at 2.0 wt. % polymer concentration, a plot of the scaled quantity $(\langle \Delta r^2(t) \rangle a)$ demonstrates that the curves for different particle sizes overlay each other over the range investigated. In addition, the characteristic Maxwell model behavior of $\langle \Delta r^2(t) \rangle$ was not observed at this concentration. The slopes of the curves at long times are ≈ 1, indicating that the particle motion is diffusive at long time for these conditions.

Results for 3.0 wt. % AP concentration are plotted in Fig. 5. For particles of size 0.3 and 0.6 μm, no obvious Maxwell model $\langle \Delta r^2(t) \rangle$ was observed. In Figs. 4–6 the reported mean square displacement data extend to different maximum times because we analyze data for $g_{(2)}(t) \geqslant 0.01$ only, as described in Sec. III D 1, and since the time required for the $g_{(2)}(t)$ to decay to the value 0.01 is a function of particle size. For larger particles (i.e., 1.1 and 2.2 μm), a modest

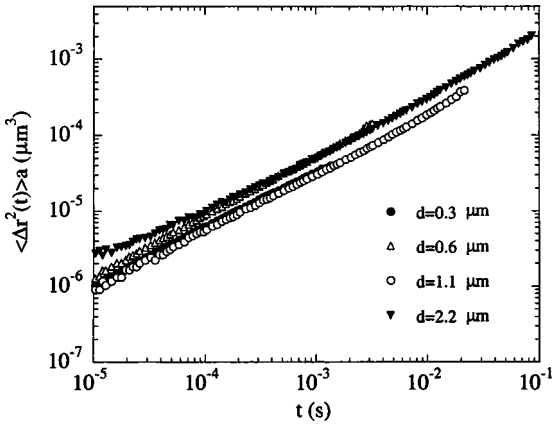

FIG. 4. The scaled quantity $(\langle \Delta r^2(t) \rangle a)$ for various probe sizes is plotted vs time. a is the radius of probe particles. The associating polymer concentration is 2.0 wt. %, the probe concentration is 1.0 vol % and $T = 25\,^{\circ}\mathrm{C}$.

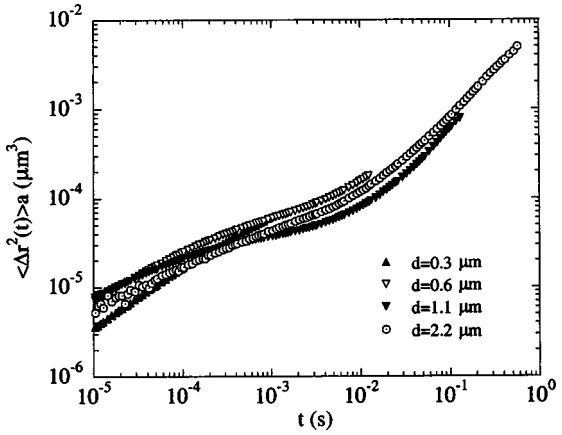

FIG. 5. $(\langle \Delta r^2(t) \rangle a)$ of various probe sizes are plotted vs time. The associating polymer concentration is at 3.0 wt. %, the probe concentration is 1.0 vol % and $T=25\,^{\circ}\mathrm{C}$.

change of slope at $t \sim 10^{-2}$ s was observed. This change roughly corresponds to the relaxation time of the polymer network, as identified by mechanical rheology (refer to Fig. 1). Again, note that at longer times, the $\langle \Delta r^2(t) \rangle$ obeys diffusive behavior.

At 4.0 wt. % AP concentration, a pronounced particle size effect in the scaled $(\langle \Delta r^2(t) \rangle a)$ appears. From Fig. 6, it is clear that this effect is most pronounced at short times. At long times, diffusive behavior is again attained. The particle size effect appears for t less than $\sim 10^{-2}$ s, which is again the approximate relaxation time of the transient AP network. At short times, the value of the scaled variable $(\langle \Delta r^2(t) \rangle a)$ is greater for larger particles. In fact, for the largest particles studied ($d=2.2\ \mu$m), the $\langle \Delta r^2(t) \rangle$ behavior approaches that of the Maxwell model prediction of Eq. (5).

The observed deviation from Maxwell model LVE becomes progressively greater as the particle size is decreased. Indeed, at the smallest particle size ($d=0.3\ \mu$m), the $\langle \Delta r^2(t) \rangle$ at short times differs from the large particle behavior by nearly a factor of 50. We note that the differences in Fig. 6 are much greater than the characteristic errors dis-

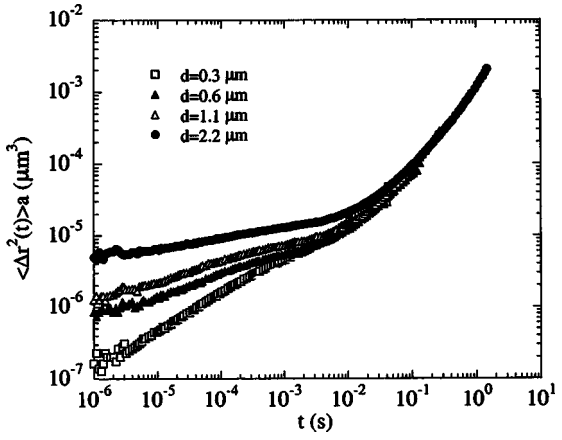

FIG. 6. $(\langle \Delta r^2(t) \rangle a)$ of various probe sizes are plotted vs time. The associating polymer concentration is 4.0 wt %. The probe concentration is 1.0 vol % and $T=25\,^{\circ}\mathrm{C}$.

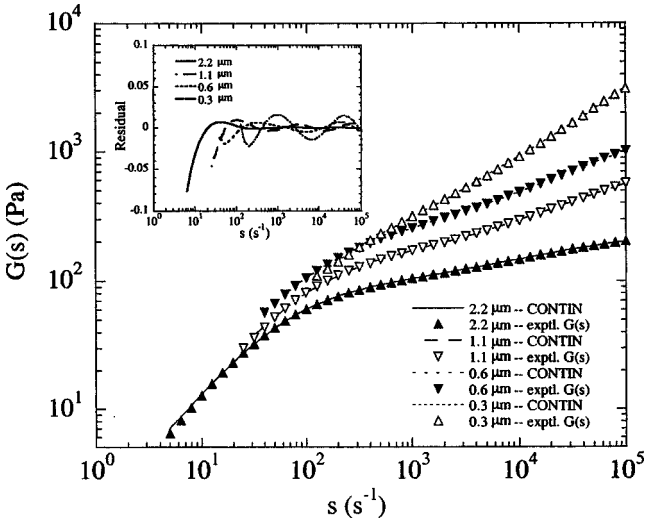

FIG. 7. Comparison between reconstructed $G(s)$ from CONTIN and the $G(s)$ calculated from the experimental mean square displacement. The inset is a plot of the fit residuals. The AP concentration is 4.0 wt. %. The probe concentration is 1.0 vol % and $T=25\,^{\circ}\mathrm{C}$.

cussed earlier (refer to the standard deviation data reported in Fig. 3). Because of these interesting results at short times, we conducted long DWS measurements ($t>10$ h) to extend our minimum sample time for this material to 10^{-6} s to confirm the finding and improve the possibility of a successful extraction of LVE from Eq. (1), as reported in the following section. The behavior of Fig. 6 is inconsistent with Eq. (1), because the observed particle size effect cannot be predicted from the generalized Stokes-Einstein equation. Since this is the first observation of a breakdown of microrheology on an associating polymer system, the results of Fig. 6 warrant further investigation, as discussed in Secs. IV C and IV D.

C. Linear viscoelastic reconstruction using CONTIN

The extraction of linear viscoelasticity from $\langle \Delta r^2(t) \rangle$ measurements allows direct comparison between microrheology and mechanical rheology. In this case, we investigate implications of Fig. 6 results for the extraction of linear viscoelastic moduli.

By applying the methods in Secs. III D 2 and III D 3, we calculate the Laplace domain shear modulus $G(s)$ from $\langle \Delta r^2(t) \rangle$ and then extract the relaxation spectra τ_i and the corresponding amplitude G_i by means of the CONTIN algorithm. The linear viscoelastic moduli are reconstructed using the relaxation spectra information. In Fig. 7, we compare the $G(s)$ reconstructed from CONTIN with $G(s)$ determined directly from experiment. In the inset of Fig. 7, we plot the residual difference between the fit and data. The maximum residuals are $\approx$7% at the lowest frequency, and for most of the data the residuals are within 2%. The fit residuals quantify that the CONTIN algorithm reconstructs the Laplace domain modulus with very high fidelity.

From the Fig. 7 spectra, $G'(\omega)$ and $G''(\omega)$ were constructed and plotted in Figs. 8 and 9, respectively. All spectra extend to $\omega=10^5\ \mathrm{s}^{-1}$. This maximum frequency corre-

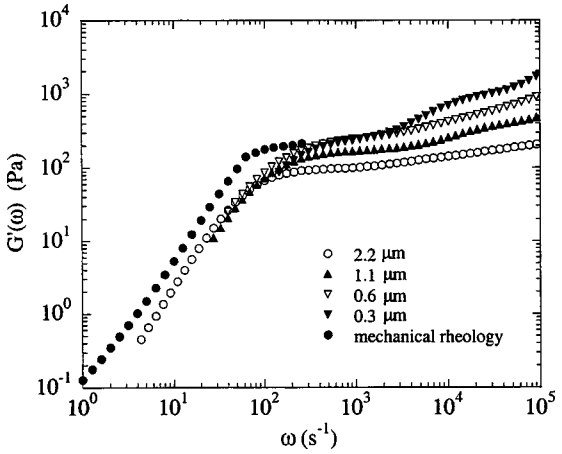

FIG. 8. Storage moduli $G'(\omega)$ of different probe sizes obtained by applying the method of Sec. III D 3. AP concentration is 4.0 wt. %. Results of mechanical rheology are also plotted.

sponds to the minimum time resolution of our data, as discussed in Sec. III D 2. Likewise, the low frequency data extend to varying limits in a way that is consistent with our selection of the cutoff $g_2(\tau) \geqslant 0.01$, as described in Sec. III D 1. Qualitative features appearing in Fig. 6 are reflected in Figs. 8 and 9. First, there is little effect of particle size for $\omega \leqslant 10^2$ s^{-1}, consistent with the long time data of Fig. 6. Second, the correct low frequency scalings $G'(\omega) \sim \omega^2$ and $G''(\omega) \sim \omega$ are apparent in the experimental data. Note that at high frequency ($\omega > 10^3$ s^{-1}), slight undulations in the $G'(\omega)$ and $G''(\omega)$ curves are observed. This behavior precisely tracks the slight functionality of the residual error in the CONTIN fit reported in the inset of Fig. 7. Thus we view these undulations as an artifact of solving the ill-posed inverse problem of Eqs. (3) and (4).

The $G'(\omega)$ and $G''(\omega)$ curves extend over a range that allows comparison to the results of mechanical rheology. Of greatest interest is the behavior of $G''(\omega)$ for $\omega > 10^2$ s^{-1}. In this range, mechanical rheology shows that $G''(\omega)$ decreases with increasing frequency. This behavior is consistent with

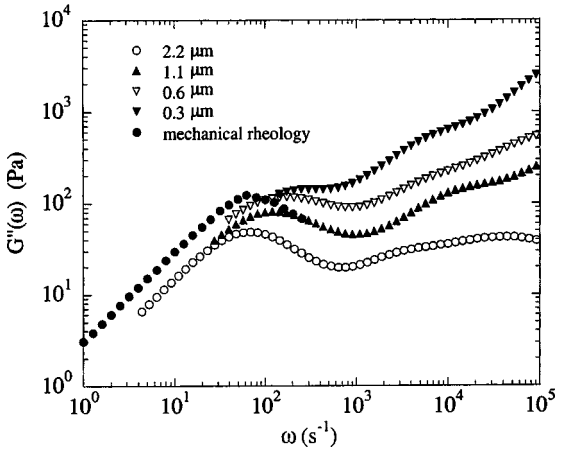

FIG. 9. Loss moduli $G''(\omega)$ of different probe sizes obtained by applying the method of Sec. III D 3. AP concentration is 4.0 wt. %. Results of mechanical rheology are also plotted.

the LVE of the single-mode Maxwell model (refer to Fig. 1). From Fig. 9, it appears that this characteristic behavior is best captured by the larger probes. This observation agrees with the results of Fig. 6, where the observed $\langle \Delta r^2(t) \rangle$ of the larger probes was most similar to the Eq. (5) prediction.

The microrheology data for $\omega > 3 \times 10^2$ s^{-1} extend beyond the range of mechanical rheology, so the extent to which these data reflect the macroscopic rheology of the material cannot be assessed at this time. However, the observed particle size effect clearly indicates that the underlying physics is more complex than allowed by Eq. (1). Interestingly, even the power law scaling exponent of $G'(\omega)$ and $G''(\omega)$ with frequency is a function of particle size. While the literature is silent regarding the expected scaling in the associating polymer systems at high frequencies, deviations from single-mode Maxwell model LVE for AP systems have been observed by high frequency mechanical rheology [49,50]. Since mechanical rheology provides no further insight into the apparent effect of probe size on the microrheology, in the following section, we report additional DWS experiments designed to further study the effect.

D. Possible origins of the particle size effect

We hypothesize that possible origins of the observed particle size effect in AP microrheology might be: (1) failure of the assumption of continuum viscoelasticity; (2) the effect of probe particle inertia; (3) compressibility of the matrix network; (4) associative polymer chain absorption on the surface of the probe particle; (5) entropic depletion of the polymer molecules in the vicinity of the particle surface; (6) structural heterogeneity of the AP network. In this section, we evaluate the possible relevance of these effects to the experimental observations.

A fundamental assumption of microrheology is the validity of continuum viscoelasticity. That is, the probe particle size should be much larger than the characteristic mesh size of the polymer network, so that the probe particles are considered to be dynamically coupled to a viscoelastic continuum (devoid of structure). Failure of this assumption would require explicit consideration of the effect of matrix structure on probe displacement. Such effects are beyond the scope of Eq. (1). For the AP solutions we studied in this research, by a radius of gyration calculation we estimated the characteristic structural size of the AP solutions to be no larger than 5–10 nm. It is reasonable to consider a ratio of probe size to matrix structural size of at least 20 as sufficient for continuum viscoelasticity to be valid [4]. Since the probe particles used in this study are of diameter 0.3 μm or greater, which is at least 30 times larger than the matrix mesh size, we expect the assumption to hold. Thus we are led to consider other possible origins of the particle size effects observed in the AP solutions.

Using the criterion of van Zanten and Rufener [15], we estimated the probe particle inertia to be significant in our system only for $t < 10^{-6}$ s. Since the particle size effects shown in Fig. 6 persist to times as long as $\sim 10^{-2}$ s, we conclude that the inertia of the probe particles cannot explain the observed behavior.

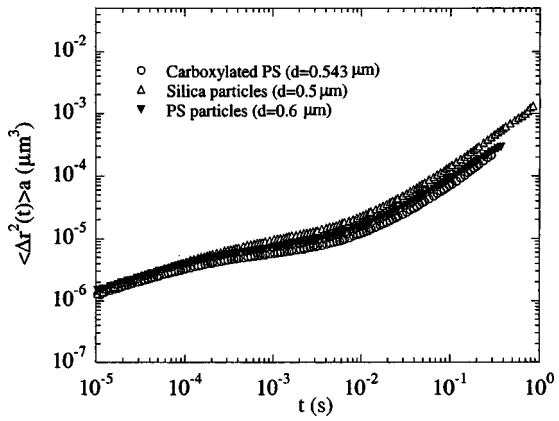

FIG. 10. $(\langle \Delta r^2(t) \rangle a)$ of different probe surface chemistry (silica particles, carboxylated polystyrene particles, and unmodified polystyrene particles) are plotted against time. The associating polymer concentration is fixed at 4.0 wt. %, the probe concentration is 1.0 vol % and $T=25\,^{\circ}\mathrm{C}$.

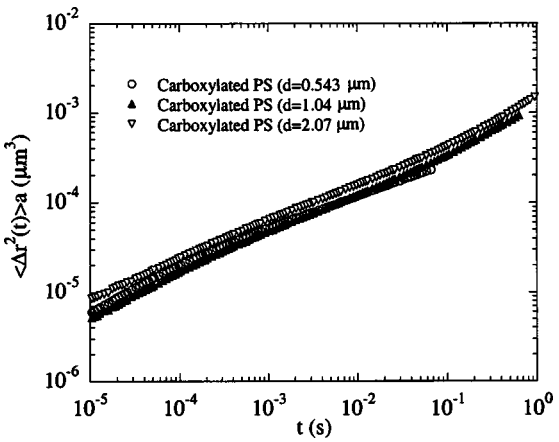

FIG. 11. $(\langle \Delta r^2(t) \rangle a)$ of various probe sizes are plotted vs time. The PEO polymer concentration is 1.5 wt. %. The molecular weight of PEO is 4.0×10^6 g/mole. The probe concentration is 1.0 vol %, with probe diameter ranging from 0.543 to 2.07 μm. Results are for $T=25\,^{\circ}\mathrm{C}$.

As first reported by Schnurr *et al.* [4] and further investigated by Levine and Lubensky [28], at low frequencies (long times) viscous drag between the AP network and solvent could lead to deviations from Eq. (1). The scaling analysis of Schnurr *et al.* [4] indicates that, for our system, such effects of network compressibility are relevant for frequencies less than of order 100 s^{-1}. This suggests that for times larger than 10^{-2} s, the effect of network compressibility may not be negligible. However, in our study the particle size effects are observed in a completely different regime: they occur for times *less than* 10^{-2} s. Thus, we conclude that this possible origin cannot account for the experimental observations.

It is possible that specific physical chemical interactions between the polymer chains and the probe surface may give rise to deviations from generalized Stokes-Einstein behavior. For example, a probe particle that is locally bound to the polymer matrix due to irreversible absorption of chains on the probe surface might undergo a thermally driven displacement inconsistent with Eq. (1). To learn if this possibility were relevant to the interpretation of the Fig. 6 results, we conducted experiments in which the surface chemistries of the probe particles were systematically varied. The following surface chemistries were studied: Silica particles ($d=0.50\,\mu$m), carboxylate-modified polystyrene spheres ($d=0.543\,\mu$m), and unmodified polystyrene spheres ($d=0.60\,\mu$m). Specific details of the surface chemistries of these particles are summarized in Sec. III B. Results are reported in Fig. 10. We find that the three different probes yield nearly identical $\langle \Delta r^2(t) \rangle$ curves. The absence of an effect of surface chemistry effect on the thermally driven displacement of the colloidal probes suggests that the specific physicochemical details of the interaction between the polymer matrix and the probe particles are not the origin of the results reported in Fig. 6.

We addressed the possibility that the Fig. 6 observations are a general behavior by investigating a different model material. We selected high molecular weight PEO because it has previously been studied by other microrheological methods [3,13]. We prepared a semidilute solution (molecular weight 4.0×10^6 g/mole, 1.5 wt. %) of PEO. The measured $(\langle \Delta r^2(t) \rangle a)$ for probe particles of different sizes are plotted in Fig. 11. As opposed to the results for the AP solutions, for semidilute PEO solutions the particle size effect was not observed, since the Fig. 10 data sets overlay for probe sizes varying from 0.543 to 2.07 μm. The comparison between the results of Figs. 6 and 11 is pivotal because it demonstrates that the breakdown of the $(\langle \Delta r^2(t) \rangle a)$ scaling predicted by Eq. (1) is not universal. Instead, the failure of Eq. (1) is apparently linked to some specific attribute of the particular AP complex fluid studied. Furthermore, the results of Figs. 6 and 11, taken together, indicate that depletion of the polymer in the vicinity of the probe surface is not the likely origin of the observed particle size effects. It is known that polymers are depleted in the vicinity of a surface to distances of order of the coil radius of gyration [51]. There has been speculation that this coil depletion would have implications for the dynamics of dispersed colloidal probes [4]. However, since depletion is a general phenomena we would expect its effect to be equally apparent in both AP and PEO solutions.

In the previous paragraphs, we have argued that the first five hypothetical origins of the Fig. 6 particle size effects are not likely relevant. We now turn our attention to the sixth possibility, structural inhomogeneity of the AP solutions. Interestingly, the literature provides ample evidence of structural inhomgeneity in associative polymer solutions. For example, microphase separation [52–54] and long-range ''super-bridging'' [29] have been reported in the AP networks. According to Klucker and Schosseler [55], fluctuations in polymer concentration can occur at a length scale an order of magnitude greater than the characteristic mesh size estimated for ideal semidilute solutions. The possibility that the structural defects in the AP solutions (i.e., inhomogeneity) are the origin of the breakdown of the $(\langle \Delta r^2(t) \rangle a)$ scaling predicted by Eq. (1) deserves further investigation.

As discussed in the Introduction, Crocker *et al.* [21] have recently demonstrated that the generalized Stokes-Einstein equation can fail for inhomogeneous complex fluids. They

proposed two-particle measurements as a method to quantify the microrheology of such materials. Therefore, further investigation of the inhomogeneity hypothesis in the AP solutions may require the execution of two-particle microrheological studies, the report of which is beyond the scope of this communication. However, we note that the possibility of structural inhomgeneity of the associative polymer solutions is not inconsistent with the Fig. 6 results. Specifically, structural inhomogeneity would tend to increase the characteristic dimension of the polymer matrix beyond that of the 5–10 nm scale of the polymer radius of gyration [55]. Thus, in a sense, the assumption of continuum viscoelasticity would be invalidated by the larger inhomogeneous regions, and the correspondence between microrheology and macroscopic rheology indicated by Eq. (1) would no longer be assured. This trend is apparent in the experimental observations: qualitatively the largest probe particle sizes studied most closely approximate the macroscopic rheological response (Figs. 6, 8, and 9), while smaller particle sizes, which are perhaps not much larger than the characteristic scale of the structural inhomogeneity, show the greatest deviations from the expected continuum viscoelastic response.

Thus, our report of the failure of the generalized Stokes-Einstein equation for the specific instance of associative polymer solutions demonstrates that the application of the powerful formalism of microrheology to this class of complex fluids requires special care. Since associative polymers can be considered to be a model of the chemically and physically heterogeneous complex fluids that are often encountered in industrial applications, the results reported here indicate that additional work is warranted to fully delineate limitations and possible extensions of microrheology so that this useful method can be more broadly applied.

ACKNOWLEDGMENTS

Support for this research was provided by the National Science Foundation (Grant No. CTS-0093076) and Dupont. We also thank Dr. S. W. Provencher for providing us with his CONTIN code.

[1] T. G. Mason and D. A. Weitz, Phys. Rev. Lett. **74**, 1250 (1995).
[2] T. G. Mason, H. Gang, and D. A. Weitz, J. Opt. Soc. Am. A **14**, 139 (1997).
[3] T. G. Mason *et al.*, Phys. Rev. Lett. **79**, 3282 (1997).
[4] B. Schnurr, F. Gittes, F. C. Mackintosh, and C. F. Schmidt, Macromolecules **30**, 7781 (1997).
[5] A. Turner and C. Hallet, Biochim. Biophys. Acta **451**, 305 (1976).
[6] G. S. Ullmann, K. Ullmann, R. M. Linder, and G. D. J. Phillies, J. Phys. Chem. **89**, 692 (1985).
[7] Z. Bu and P. S. Russo, Macromolecules **27**, 1187 (1994).
[8] J. C. Reina, R. Bansil, and C. Konak, Polymer **31**, 1038 (1990).
[9] J. Won, C. Onyenemezu, W. G. Miller, and T. P. Lodge, Macromolecules **27**, 7389 (1994).
[10] V. S. Volkov and A. I. Leonov, J. Chem. Phys. **104**, 5922 (1996).
[11] A. R. Bausch, W. Moller, and E. Sackmann, Biophys. J. **76**, 573 (1999).
[12] E. Helfer *et al.*, Phys. Rev. Lett. **85**, 457 (2000).
[13] A. Palmer, J. Xu, and D. Wirtz, Rheol. Acta **37**, 97 (1998).
[14] F. Cardinaux, L. Cipelletti, F. Scheffold, and P. Schurtenberger, Europhys. Lett. **57**, 738 (2002).
[15] J. H. van Zanten and K. P. Rufener, Phys. Rev. E **62**, 5389 (2000).
[16] T. Gisler and D. A. Weitz, Curr. Opin. Colloid Interface Sci. **3**, 586 (1998).
[17] F. C. MacKintosh and C. F. Schmidt, Curr. Opin. Colloid Interface Sci. **3**, 391 (1998).
[18] A. Mukhopadhyay and S. Granick, Curr. Opin. Colloid Interface Sci. **6**, 423 (2001).
[19] M. J. Solomon and Q. Lu, Curr. Opin. Colloid Interface Sci. **6**, 430 (2001).
[20] J. L. Harden and V. Viasnoff, Curr. Opin. Colloid Interface Sci. **6**, 438 (2001).
[21] J. C. Crocker *et al.*, Phys. Rev. Lett. **85**, 888 (2000).
[22] H. Ma, J. Jimenez, and R. Rajagopalan, Langmuir **16**, 2254 (2000).
[23] G. Popescu, A. Dogariu, and R. Rajagopalan, Phys. Rev. E **65**, 041504 (2002).
[24] D. Weitz and D. Pine, in *Dynamic Light Scattering, The Method and Some Applications*, edited by W. Brown (Clarendon Press, Oxford, 1993), p. 652.
[25] D. J. Pine, D. A. Weitz, P. M. Chaikin, and E. Herbolzheimer, Phys. Rev. Lett. **60**, 1134 (1988).
[26] B. Schnurr *et al.*, in *Grain Boundaries in Semiconductors*, edited by H. J. Leamy, G. E. Pike, and C. H. Seager, Mater. Res. Soc. Symp. Proc. No. 5 (Materials Research Society, Pittsburgh, 1982), p. 463.
[27] A. J. C. Ladd, H. Gang, J. X. Zhu, and D. A. Weitz, Phys. Rev. E **52**, 6550 (1995).
[28] A. J. Levine and T. C. Lubensky, Phys. Rev. Lett. **85**, 1774 (2000).
[29] T. Annable, R. Buscall, R. Ettelaie, and D. Whittlestone, J. Rheol. **37**, 695 (1993).
[30] M. A. Winnik and A. Yekta, Curr. Opin. Colloid Interface Sci. **2**, 424 (1997).
[31] K. C. Taylor and H. A. Nasr-El-Din, J. Pet. Sci. Eng. **19**, 265 (1998).
[32] S. Mechen and B. Johnson, Chem. Mater. **8**, 2205 (1996).
[33] K. C. Tam, R. D. Jenkins, M. A. Winnik, and D. R. Bassett, Macromolecules **31**, 4149 (1998).
[34] G. Marrucci, S. Bhargava, and S. L. Cooper, Macromolecules **26**, 6483 (1993).
[35] R. Larson, *The Structure and Rheology of Complex Fluids* (Oxford University Press, New York, 1999), p. 248.
[36] B. Xu *et al.*, Langmuir **13**, 2447 (1997).
[37] S. K. Kumar and J. F. Douglas, Phys. Rev. Lett. **87**, 188301 (2001).
[38] T. G. Mason *et al.*, J. Rheol. **44**, 917 (2001).

[39] J. P. Kaczmarski and J. E. Glass, Macromolecules **26**, 5149 (1993).
[40] W. Stober, A. Fink, and E. Bohn, J. Colloid Interface Sci. **26**, 62 (1968).
[41] G. H. Bogush, M. A. Tracy, and M. A. Zukoski IV, J. Non-Cryst. Solids **104**, 95 (1988).
[42] H. C. van de Hulst, *Light Scattering by Small Particles* (Dover, New York, 1981), Chap. 9.
[43] C. S. Johnson and D. A. Gabriel, *Laser Light Scattering* (Dover, New York, 1994), p. 32.
[44] S. W. Provencher, Comput. Phys. Commun. **27**, 213 (1982).
[45] S. W. Provencher, Comput. Phys. Commun. **27**, 229 (1982).
[46] J. D. Ferry, in *Viscoelastic Properties of Polymers*, 3rd ed. (Wiley, New York, 1981).
[47] P. Stepanek, in *Dynamic Light Scattering, The Method and Some Applications*, edited by W. Brown (Clarendon Press, Oxford, 1993), Chap. 4.
[48] D. W. Mead, J. Rheol. **38**, 1769 (1994).
[49] W. K. Ng, K. C. Tam, and R. D. Jenkins, J. Rheol. **44**, 137 (2000).
[50] B. Xu *et al.*, Colloids Surf., A **112**, 239 (1996).
[51] J. N. Israelachvili, *Intermolecular and Surface Forces*, 2nd ed. (Academic, San Diego, CA, 1992), p. 299.
[52] Q. T. Pham, W. B. Russel, J. C. Thibeault, and W. Lau, Macromolecules **32**, 2996 (1999).
[53] Q. T. Pham, W. B. Russel, J. C. Thibeault, and W. Lau, J. Rheol. **43**, 1599 (1999).
[54] A. N. Semenov, J. F. Jaonny, and A. R. Khokhlov, Macromolecules **28**, 1006 (1995).
[55] R. Klucker and F. Schosseler, Macromolecules **30**, 4927 (1997).